2008 IEEE International Conference on
Robotics and Automation
Pasadena, CA, USA, May 19-23, 2008

An easy calibration for oblique-viewing endoscopes

Chenyu Wu and Branislav Jaramaz

Abstract— **Oblique-viewing endoscopes (oblique scopes) are widely used in minimally invasive surgery. The viewing direction of an oblique endoscope can be changed by rotating the scope cylinder, which enables a larger field of view, but makes the scope calibration process more difficult. The calibration is a critical step for incorporating oblique scope into computer assisted surgical procedures (robotics, navigation, augmented reality), though few calibration methods of oblique endoscopes has been developed. Yamaguchi et al. [1] first modelled and calibrated the oblique scope. They directly tracked the camera head and formulated the scope cylinder's rotation to the camera model as an extrinsic parameter. Their method requires five additional parameters to be estimated. In this work, we track the scope cylinder instead. Since the rotation of the camera head with respect to the cylinder only causes the rotation of the image plane, less parameter needs to be estimated. Experiments demonstrate the ease, simplicity and accuracy of our method.**

I. INTRODUCTION

One of the main goals of computer assisted orthopedic surgery is to enable true minimally invasive surgery (MIS). As a key MIS tool, endoscope is attracting increasing attention for its potential role in computer assisted surgery, especially in surgical navigation. By tracking the endoscope in space using a position localizer, its function can be significantly augmented. For example, it can be used to create augmented reality systems, fusing the virtual and real endoscopic images [2], to map real endoscopic images onto anatomic surfaces derived from CT images [3], or to recover the 3D shape from a single endoscopic image [4], [5] or from multiple images [6], [7], [8]. Camera calibration, as an important step in endoscope related applications, is mostly based on Tsai's model [9] (which has been addressed in several work, including [1], [3], [10], [11]. However, except [1], most of these methods deal with the hand-eye calibration of the forward-viewing endoscope, in which the viewing direction is aligned with the axis of the endoscope. Due to the constraints of the small incision, the range of movement of such a tool is restricted. In order to view sideways, oblique scope has been designed to have a tilted viewing direction, and a wider viewing field could be reached by rotating the scope cylinder. Fig. 1 illustrates an oblique-viewing endoscope. Rotation happens between the scope cylinder and the camera head.

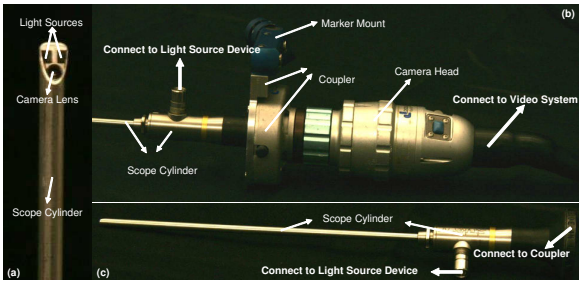

Fig. 1. An oblique endoscope consists of a scope cylinder with a lens and point light sources at the tip (the tip has a tilt from the scope cylinder), a camera head that captures video images, and a light source device that supports the illumination. Scope cylinder is connected to the camera head via a coupler. This connection is flexible such that you can rotate either the scope cylinder or the camera head separately, or rotate them together.

Yamaguchi et al. first modelled and calibrated oblique-viewing endoscopes [1], [12]. They attached an optical marker onto the camera head and formulated the rotation angle of the scope cylinder as another external parameters in Tsai's camera model. In the first step they applied Tsai's camera model to the scope with zero rotation and estimate the transformation from camera to the marker. Next when the cylinder of the scope is rotated by θ , two more transformations are added to compensate the rotation of the lens system with respect to the camera head. Since these two transformations are basically two rotations around different axes by θ , four parameters need to be estimated. Finally in order to estimate θ, they use a rotary encoder attached to the camera head.

Yamaguchi et al's camera model successfully compensates the rotation effect but their method requires five additional parameters and the model is complicated. In this work we propose an alternative approach to simplify the calibration. We attach an optical marker to the scope cylinder instead of the camera head, with a newly designed coupler (as Fig. 1(b) illustrates). When there is no rotation between the camera head and the scope cylinder, we can still use Tsai's model to do the calibration. When the rotation happens, the transformation from the lens system to the marker is fixed and not affected by the rotation angle. Based on our observation, the only change is that the image plane will rotate around the principal point by the same angle. Since principal point is the intrinsic parameter that has been estimated in the first step. Thus, we only need to estimate the rotation angle θ. In order to find the rotation angle, we use two optical markers when the rotary encoder is absent.

This work was supported in parts by an NSF Grant 0325920 ITR: Data-driven Human Knee Modeling for Expert Surgical Planning Systems

Chenyu Wu is with Robotics Institute, School of Computer Science, Carnegie Mellon University, Pittsburgh, PA 15213, USA chenyuwu@cmu.edu

Branislav Jaramaz is with Faculty of Robotics Institute, School of Computer Science, Carnegie Mellon University, Pittsburgh, PA 15213, USA. He is also the Director of Institute for Computer Assisted Orthopaedic (ICAOS) Surgery, Western Pennsylvania Hospital, Mellon Pavilion - Suite 242, Pittsburgh, PA 15224, USA branko@icaos.org

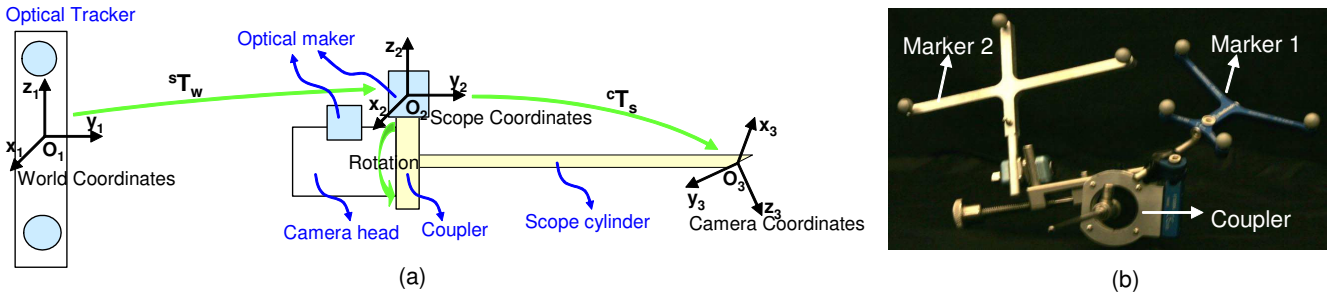

Fig. 2. The geometric model of endoscope based on a tracking system. A new coupler (see Fig. 1 (b))is designed to mount an optical marker to the scope cylinder which ensures that the transformation from scope(marker) coordinates O_2 to the lens system (camera) coordinates O_3 is fixed. World coordinates O_1 is defined by the optical tracker. Two optical markers are attached to the coupler and camera head separately in order to compute the rotation θ in between.

We have two contributions in this work. We first develop a simpler camera model for oblique-viewing endoscopes than Yamaguchi et al.'s work. Less additional parameter needs to be estimated. Next, we propose to use two markers to estimate the rotation angle, instead of a rotary encoder. Since the optical marker is easier to obtain than the rotary encoder in surgical navigation systems based the discussion with surgeons, our method is more practical for surgery.

II. METHOD

Orthopedic endoscopes have a single camera and one or more point light sources equipped at the tip of the scope. For this work, we use two oblique endoscopes as examples. One of them is shown in Fig. 1 and another one is in Fig. 6.

A. Model for Oblique-viewing Endoscope

Yamaguchi et al's camera model is based on Tsai's model [9], [10]:

$$\begin{aligned} \lambda p_i &= A \cdot {}^cT_m(\theta) \cdot {}^mT_w \cdot P_w \\ {}^cT_m(\theta) &= T_R(-\theta; l_h(\theta)) T_R(\theta; l_s) {}^cT_m(0) \end{aligned} \tag{1}$$

where P_w is a 3D point in the world coordinates, p_i is the corresponding 2D image pixel. ${}^mT_w$ is a rigid transformation from the world coordinates to the optical marker coordinates, ${}^cT_m(\theta)$ is a rigid transformation from the marker (camera head) to the camera coordinates. ${}^cT_m(\theta)$ is dependent on the rotation angle θ. By considering the marker coordinates (camera head) as a reference, only the lens system rotates while the camera head, i.e., the image plane, remains fixed irrespective of the rotation. They describe such a transformation due to the rotation by decomposing the one physical rotation into two mathematical rotations. $T_R(\theta; l_s)$ is a rotation of both scope cylinder and the camera head (image plane) around the axis of cylinder l_s. $T_R(-\theta; l_h(\theta))$ is an inverse rotation of the image plane around the z-axis of lens system l_h. Both l_s and l_h have two unknown parameters. Although this model works well, it is very complicated.

As Fig. 2 shows, in our work, we attach an optical marker on the scope cylinder instead. Our model is still an extension of Tsai's model, the geometric model illustrated in Fig. 2 (a) can be written as:

$$\begin{aligned} \lambda p'_i &= A \cdot {}^cT_m \cdot {}^mT_w \cdot P_w \\ p_i &= R(\theta) \cdot (p'_i - cc) + cc \end{aligned} \tag{2}$$

where P_w is a 3D point in the world coordinates, p'_i is the corresponding 2D image pixel without rotation, p_i is the image pixel with rotation θ. ${}^mT_w$ is a rigid transformation from world coordinates to the optical marker coordinates, ${}^cT_m$ is a rigid transformation from the marker (scope cylinder) to the camera coordinates and independent on θ. cc is the principal point which is an intrinsic parameter. $R(\theta)$ represents a rotation of the image plane around cc by θ. Thus camera intrinsic matrix A and external matrix ${}^cT_m$ can be calibrated by using Zhang's method [10] and ${}^mT_w$ can be obtained directly from the tracking system. In our model we only need to estimate the rotation angle. Ymaguchi et al.'s method needs to estimate the misalignment between the scope and camera image plane since their model involve physical rotations. However, in our model we simultaneously estimate the intrinsic and extrinsic parameters without assuming anything about camera coordinates. Misalignment will be included in the estimation of intrinsic and extrinsic parameters. Thus we do not need to estimate other parameters as Ymaguchi et al. did.

Rotation angle can be estimated by using a rotary encoder, as Yamaguchi et al [12] did. When it is absent, the rotation angle can be estimated by using two optical markers: one attached to the scope cylinder and the other one on the rod (camera head).

A comparison between our model and Yamaguchi et al's model is listed in Fig. 3. Yamaguchi et al's use the camera head as a reference coordinates in their hand-eye calibration system. Since surgeons rotate the scope cylinder with respect to the camera head in order to view sideways, it is a natural way to consider the camera head as a reference. However it makes the cameral model very complex. To think in an opposite way, no matter how surgeons rotate the scope cylinder, if the reference coordinates is on the cylinder, the lens system is fixed with respect to the cylinder but the camera head rotates around θ. Thus the external parameters are not affected by the rotation anymore. Since the image

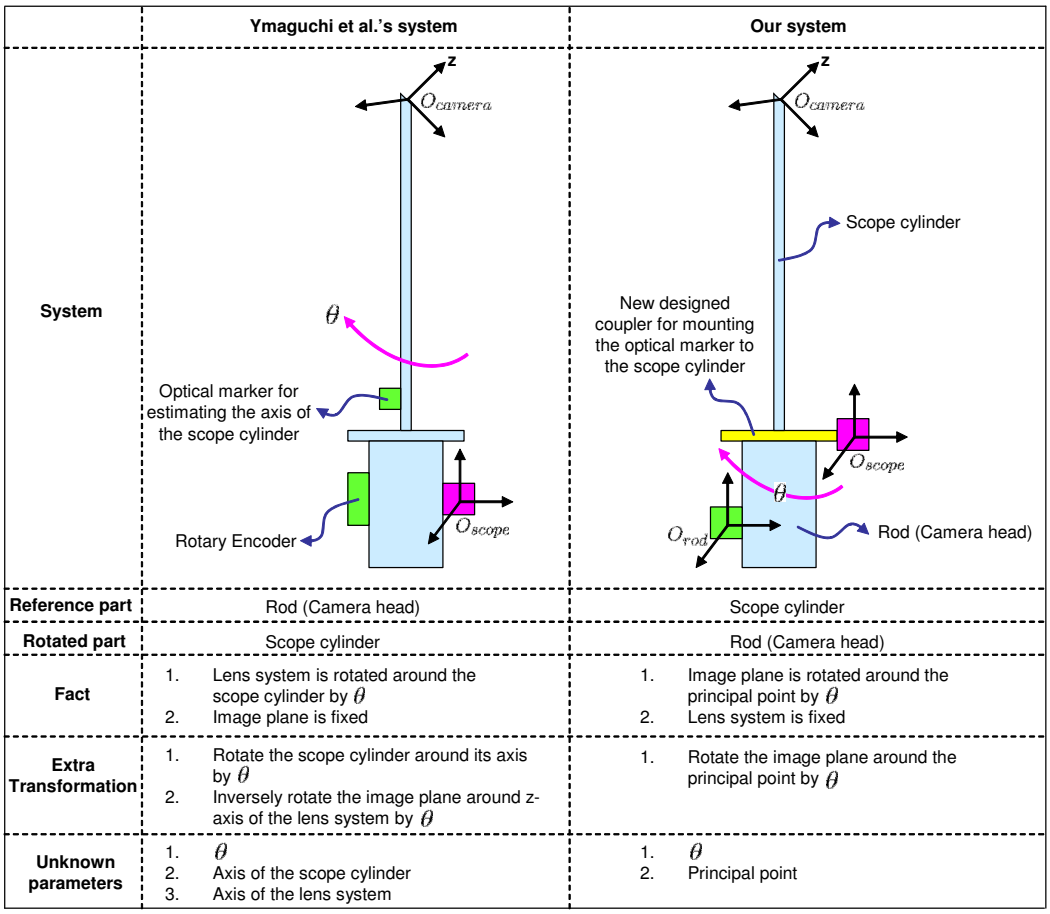

Fig. 3. A comparison between Yamaguchi et al.'s system and ours. In Yamaguchi et al.'s system, the camera head is tracked such that the transformation from the marker to the lens system is not fixed but depends on the rotation angle θ. Let the marker coordinates as a reference, the lens system is rotated around the scope cylinder about θ, but the image plane (that is in the camera head) remains the same. They use two additional transformation to describe the effect of rotation, so their model becomes complicated. Moreover, they need to calibrate the axis of both the scope cylinder and the lens system by using another optical maker attached to the scope cylinder. Based on our observation, it is possible to simplify the model if we fix the transformation between the marker and the lens system. We design a coupler that enables the mounting of the optical marker onto the scope cylinder. Then we set the marker coordinates as a reference, the lens system is fixed. The rotation only affects the image plane since the camera head is rotated around the cylinder (reference). And the image plane only rotates around the principal point. Since the principal point is an intrinsic parameter, we only need to estimate the rotation angle. As a result, we come up with a very simple model (see details in the text).

plane is in the camera head, the rotation only affects the image plane. Our method is therefore developed based on above observations. Yamaguchi et al.'s model needs five more parameters but we need less (only rotation angle). They use two optical markers and one rotary encoder. We only need two optical markers.

B. Estimate Rotation Angle Using Two Optical Markers

Let the marker attached to the scope cylinder be Marker 1 and the marker to the rod (camera head) be Marker 2 (Fig. 2 (b)). As Fig. 4 shows, when we rotate the camera head around the scope cylinder by θ, point P_r in Marker 2's coordinates O_2 will move along a circle with respect to a point O on the axis of the scope cylinder, in Marker 1's coordinates O_1. Thus we can estimate the center O of the circle first and compute θ as:

$$\theta = \arccos \frac{\|O\vec{P}_r^A\|^2 + \|O\vec{P}_r^B\|^2 - \|P_r^A\vec{P}_r^B\|^2}{2\|O\vec{P}_r^A\| \cdot \|O\vec{P}_r^B\|} \quad (3)$$

The center of the circle can be represented in terms of the transformation from the world coordinates O_w to Marker 1's coordinates O_1 and Marker 2's coordinates O_2, and at least 3 different positions of Marker 2 (O_2) (with different θ) are necessary.

C. Estimation of the center of circle in 3D

We rotate the camera head around the cylinder to acquire 3 different positions of Marker 2. Let the transformation matrix from the world coordinates O_w to both Marker 1's coordinates O_1 and Marker 2's coordinates O_2 for position i be $({}^{o_1}T_{o_w}{}^{i}, {}^{o_2}T_{o_w}{}^{i})$ $(i = 1, 2, 3)$. Given any point $\vec{P}_r$ in O_2, we first compute the position $\vec{P}_i$ in O_1 corresponding to different rotations as:

$$\vec{P}_i = {}^{o_1}T_{o_w}{}^{i} \cdot ({}^{o_2}T_{o_w}{}^{i})^T \cdot \vec{P}_r, i = 1, 2, 3. \quad (4)$$

Therefore, O is the center of the circumcircle of the triangle ($\vec{P}_1$, $\vec{P}_2$ and $\vec{P}_3$).

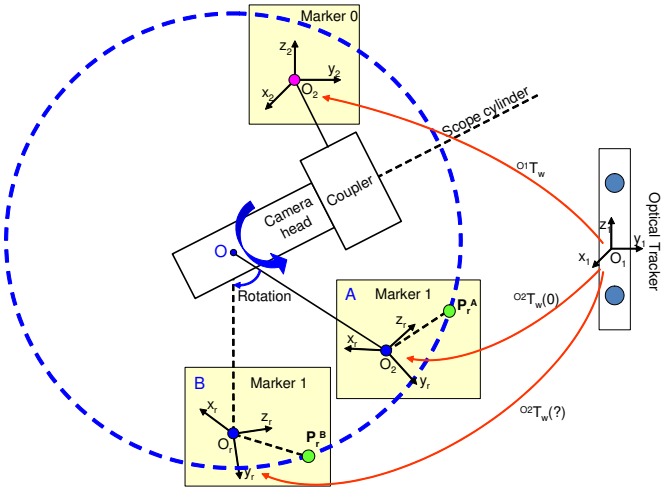

Fig. 4. Illustration of the relationship between the rotation angle θ and two marker coordinates. (O_1 is attached to the scope cylinder and O_2 is attached to the camera head. A indicates the position of O_2 when $\theta = 0$ and B indicates the position of O_2 given a rotation θ. Given any point P_r in O_2, its trace with the rotation of the camera head is a circle in Marker 1's coordinates O_1. It moves from position P_i^A to P_i^B in Marker 1's coordinates O_1. This circle is also on the plane perpendicular to the axis of scope cylinder. O is the center of the circle.

Let $\vec{R_1} = \vec{P_1} - \vec{P_3}$, $\vec{R_2} = \vec{P_2} - \vec{P_3}$, the normal of the triangle is $\vec{n} = \vec{R_1} \times \vec{R_2}$. The perpendicular bisector $\vec{L_1}$ of $\vec{R_1}$ and $\vec{L_2}$ of $\vec{R_2}$ can be computed as:

$$\begin{aligned} \vec{L_1} &= \vec{P_3} + \vec{R_1}/2 + \lambda_1 \cdot \vec{n} \times \vec{R_1} \\ \vec{L_2} &= \vec{P_3} + \vec{R_2}/2 + \lambda_2 \cdot \vec{n} \times \vec{R_2} \end{aligned} \tag{5}$$

where λ_1 and λ_2 are parameters of the line $\vec{L_1}$ and $\vec{L_2}$. The intersection of these two lines are the center of the circle. From Equation 5 we can derive the center of the circle as:

$$\vec{O} = \frac{(\vec{R_2} - \vec{R_1}) \cdot \vec{R_1}/2}{\mid \vec{R_1} \times \vec{R_2} \mid^2} \cdot (\vec{R_1} \times \vec{R_2}) \times \vec{R_2} + \vec{R_2}/2 + \vec{P_3} \tag{6}$$

It can be easily proved that O does not depend on the selection of $\vec{P_r}$. Since at least 3 different positions are necessary, we rotate the camera head around the scope cylinder by N different angles. We then apply a RANSAC algorithm to estimate $\vec{O}$ using random positions, and select $\tilde{\vec{O}}$ which corresponds to the smallest variance as the center of the circle. The pseudo code of RANSAC is listed in Table I. It can be also proved that θ does not depend on the selection of P_r either. A similar RANSAC algorithm as Table II shows is then used to compute θ. Fig. 5 shows the estimated rotation angle using RANSAC algorithm for two different endoscopes. The red curves are output angles from different RANSAC iterations, the black curve is the average angle. We can see the variance of the estimation is very small (less than 0.2 degree).

III. Experimental Results

We tested our algorithm using two different systems. We first tested it in our lab. We used Stryker 344-71 arthroscope

TABLE I

Pseudo code of RANSAC for estimating the center of the circle

Loop k=1:K (K=2000)
Generate a random point P_r from 3D space
Generate random number x,y,z between [1,N]
Compute P_x,P_y,P_z using Eq. 4
Compute O_k using Eq. 6
Compute $\mid \overline{O_k P_j} \mid, j \in [1, N], j \neq x, y, z$
Compute v_k
Save O_k, v_k
End loop
Return $O_q, q = arg_k min(v_k)$

TABLE II

Pseudo code of RANSAC for estimating the rotation angle

Loop k=1:K (K=1000)
Generate a random point P_r from 3D space
Compute P_A and P_B using Eq. 4
Compute θ_k using Eq. 3
End loop
Return $\theta = \frac{1}{K} \sum_k \theta_k$

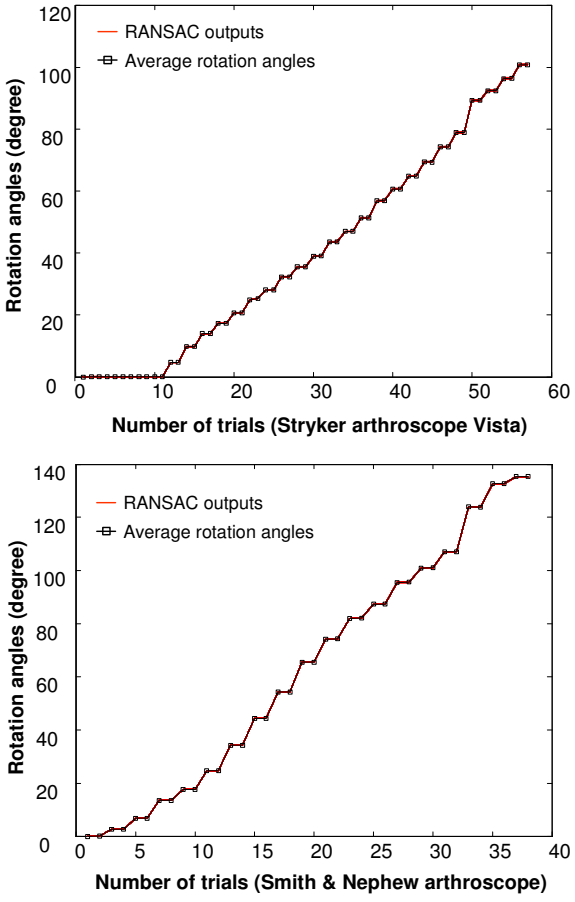

Fig. 5. Estimated rotation angles for two endoscopes. In each trial we rotated the camera head with respect to the scope cylinder and captured an image. We captured a few images for the initial position. After that we took two images for each rotation angle. The red curves are estimated rotation angles from different RANSAC iterations. The black curve indicates the average rotation angle based on all RANSAC trials.

Vista (70 degree, 4mm) oblique-viewing endoscope, DYONICS DyoCam^{TM} 750 video camera, DYONICS DYOBRITE 3000 light source, Polaris (Northern Digital Inc., Ontario, Canada) optical tracker. Next we tested it in the operating room. We used Smith & Nephew video arthroscope - autoclavable SN-OH 272589 (30 degree, 4mm), DYONICS video camera and light source, OPTOTRAK (Northern Digital Inc., Ontario, Canada) optical tracker. Fig. 6 shows the different endoscopes and optical trackers.

The endoscope was first fixed and the calibration pattern was rotated on the table for capturing images. A set of images were captured without a rotation between the scope cylinder and camera head. They were used to estimate both the intrinsic matrix A (including focal length and radial distortion coefficients) and extrinsic matrix ${}^{c}T_{m}$ using Zhang's method [10] (implemented using OpenCV functions). After that, when there was a rotation happening between the camera head and the scope cylinder, another set of images were captured and the center of the circle can be computed by using Eq. 6. Next, we fixed the calibration pattern, with two optical markers attached to the scope cylinder and the camera head, we captured a set of images by applying general motions of the endoscope (moving the whole scope body or rotating the camera head with respect to the scope cylinder (or more natural description: rotating the scope cylinder with respect to the camera head)). This set of images were used to estimate the rotation angles. The initial position of the camera head was considered as the reference position A illustrated in Fig. 4. Fig. 7 illustrates the back projection of 3D corners of the calibration pattern with (blue) and without (red) a rotation compensation. Green points are ground truth. For each rotation angle of the endoscope, we computed the average back projection error for this angle as:

$$\epsilon(\theta) = \frac{1}{M}\sum_{i=1}^{M} \mid p_i - p(P_i, \theta) \mid \qquad (7)$$

where P_i is a 3D point in the world coordinates, p_i is the corresponding 2D image pixel, $p(P_i, \theta)$ is the back projected 2D image pixel of P_i. M is the number of corners on the calibration pattern. We have used different grid patterns (3x4 as shown in Fig. 7, 4x5 and 5x6. The size of each checker is 2mm x 2mm). In order to obtain enough light on the grid pattern, the endoscope needs to be placed very close to the target (usually 5-15mm). So the smaller grid cannot capture the radial distortion but the bigger grid will exceed the field of view. The 5x6 grid gave the best results.

Finally we did many trials by moving and rotating the endoscope randomly and estimate θ simultaneously. The average back projection error with respect to the different rotation angles are shown in Fig. 8. Fig. 8 (a) is the result using Stryker 344-71 arthroscope Vista (70 degree, 4mm) and Polaris optical tracker. Fig. 8 (b) is the result using Smith & Nephew video arthroscope - autoclavable SN-OH 272589 (30 degree, 4mm) and OPTOTRAK optical tracker. The red curve represents the back projection error without taking into account of the rotation angle, and the blue curve

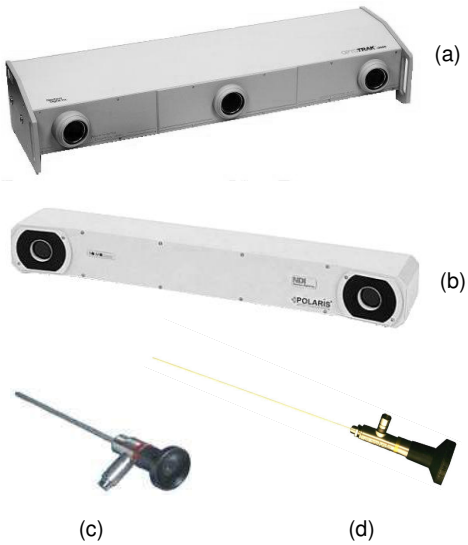

Fig. 6. Optical trackers and endoscopes used in the experiments. (a) OPTOTRAK optical tracker (Northern Digital Inc., Ontario, Canada). (b) Polaris optical tracker (Northern Digital Inc., Ontario, Canada). (c) Smith & Nephew video arthroscope - autoclavable SN-OH 272589 (30 degree, 4mm). (d) Stryker 344-71 arthroscope Vista (70 degree, 4mm).

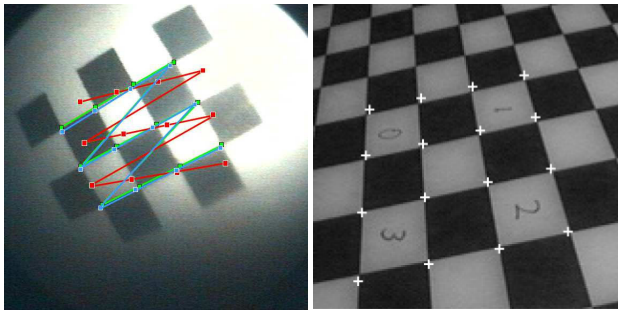

Fig. 7. (a) Illustration of the back projection with and without a rotation compensation. Green points are ground truth - 2D corner pixels on the image of the calibration pattern. Red points are back projection of the 3D world positions of the corners using the first equation of Eq. 2, which has no rotation compensation. Blue points are back projection using both equations of Eq. 2. Since the rotation is included in the camera model, the back projected pixels are much closer to the ground truth than the red points. (b) An image used in Yamaguchi et al. [1], [12]'s paper. This image has a higher resolution, better lighting and less distortion than ours.

shows the error with considering the rotation angle. The results show that including the rotation angle into the camera model significantly improve the accuracy of the calibration.

Fig. 8 shows that final calibration accuracy depends on the magnification of endoscopes and accuracy of optical trackers (according to the manufacturer, RMS error is 0.1mm for OPTOTRAK and 0.3mm for Polaris). Yamaguchi et al. [1], [12] used an OTV-S5C laparoscope (Olympus Optical Co. Ltd., Tokyo, Japan) and Polaris optical tracker. They have achieved a high accuracy of less than 5mm back projection error when the rotation angle is within 140 degrees. Our results show that we can achieve the same level accuracy

when the rotation angle is within 75 degrees. Beyond this range, due to the bigger magnification, larger radial distortion and poorer lighting (a comparison between images used in our experiment and Yamaguchi et al.'s experiment is shown in Fig. 7), the back projection error is increased to 13mm when the rotation angle is 100 degrees. When given the same quality endoscopes, we should be able to achieve the same level of accuracy.

IV. Conclusion

In this paper we propose a new method to calibrate oblique viewing endoscopes. Based on our knowledge only Yamaguchi et al. [1], [12] has worked on this topic. Compared with their method, we simplify the geometric model by attaching the optical marker to the scope cylinder instead of the camera head, which makes the calibration much simpler and more straightforward. In order to estimate the rotation angle, Yamaguchi et al. suggested to use a rotary encoder. When such a device is absent, we propose to use two markers to estimate the rotation angle. Experimental results show that our method is easy and practical for real surgery. Even with poor quality endoscopes, our method can still achieve a good accuracy.

V. Acknowledgments

The authors want to thank James Moody for design of coupling, ICAOS (Institute for Institute for Computer Assisted Orthopaedic Surgery) for help in data collection.

References

[1] T. Yamaguchi, M. Nakamoto, Y. Sato, Y. Nakajima, K. Konish, M. Hashizume, T. Nishii, N. Sugano, H. Yoshikawa, K. Yonenobu, and S. Tamura, "Camera model and calibration procedure for oblique-viewing endoscope," in *Proc. of MICCAI'03*, vol. LNCS 2879, 2003, pp. 373–381.

[2] M. J. Clarkson, D. Rueckert, A. P. King, P. J. Edwards, D. L. G. Hill, and D. J. Hawkes, "Registration of video images to tomographic images by optimising mutual information using texture mapping," in *Proc. of MICCAI'99*, vol. LNCS 1679, 1999, pp. 579–588.

[3] D. Dey, D. G. Gobbi, P. J. Slomka, K. J. Surry, and T. M. Peters, "Automatic fusion of freehand endoscopic brain images to three-dimensional surfaces: creating stereoscopic panoramas," *IEEE Trans. on Medical Imaging*, vol. 21, no. 1, pp. 23–30, 2002.

[4] K. Deguchi and T. Okatani, "Shape reconstruction from an endoscope image by shape-from-shading technique for a point light source at the projection center," in *Proc. of IEEE MMBIA'96*, 1996, pp. 290–298.

[5] C. H. Q. Forster and C. L. Tozzi, "Towards 3d reconstruction of endoscope images using shape from shading," in *Proc. of XIII Brizilian Symposium on Computer Graphics and Image Processing*, 2000, pp. 90–96.

[6] F. Mourgues and Ève Coste-Manière, "Flexible calibration of actuated stereoscopic endoscope for overlay in robot asssisted surgery," in *Proc. of MICCAI'02*, 2002, pp. 25–34.

[7] D. Stoyanov, A. Darzi, and G. Z. Yang, "A practical approach towards accurate dense 3d depth recovery for robotic laparoscopic surgery," *Computer Aided Surgery*, vol. 10, no. 4, pp. 199–208, 2005.

[8] C. Wengert, M. Reeff, P. C. Cattin, and G. Székely, *Fully Automatic Endoscope Calibration for Intraoperative Use*. Bildverarbeitung für die Medizin, Springer-Verlag, 2006 March.

[9] R. Y. Tsai, "A versatile camera calibration technique for high-accuracy 3d machine vision metrology using off-the-shelf tv cameras and lenses," *IEEE Journal of Robotics and Automation*, vol. RA-3, pp. 323–344, 1987.

[10] Z. Zhang, "A flexible new technique for camera calibration," Microsoft Research, Tech. Rep. MSR-TR-98-71, 1998.

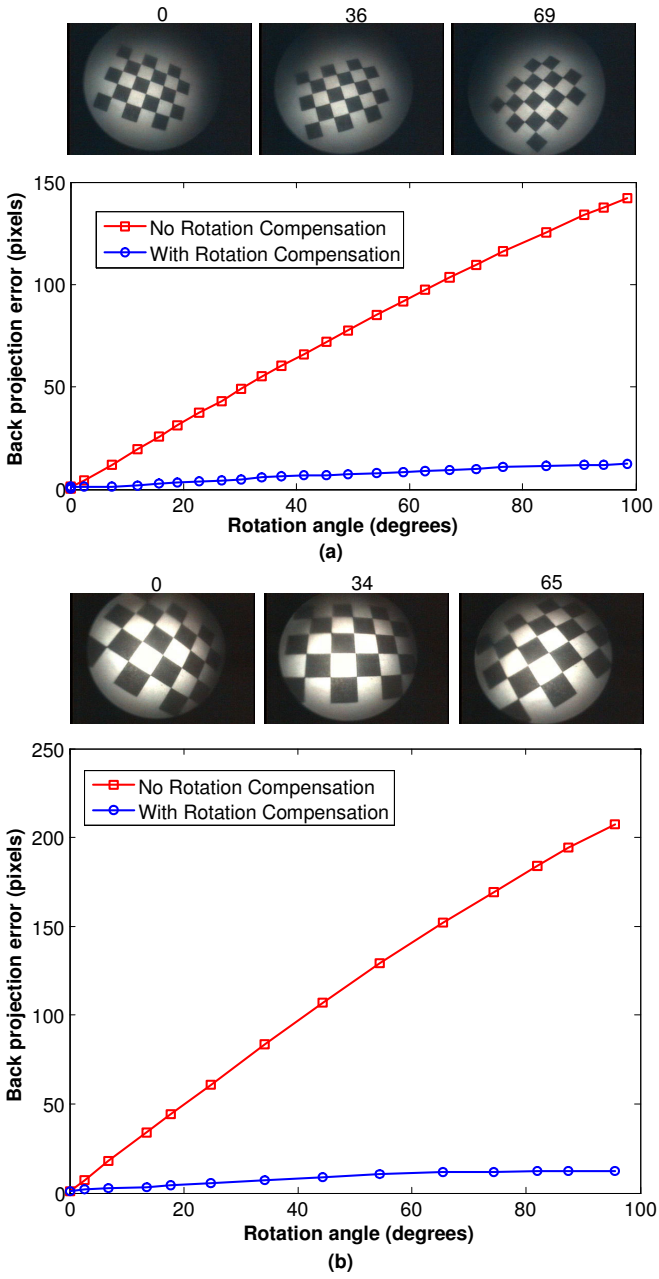

Fig. 8. Back projection errors with respect to the rotation angles for two systems. (a) Stryker 344-71 arthroscope Vista and Polaris optical tracker in our lab. (b) Smith & Nephew video arthroscope and OPTOTRAK optical tracker in the operating room. Images in the top row of (a) and (b) correspond to different rotation angles (the number is shown on the top of each image). The red curves in (a) and (b) represent the errors without a rotation compensation. The blue curves in (a) and (b) are errors with a rotation compensation.

[11] R. Shahidi, M. R. Bax, C. R. Maurer, J. A. Johnson, E. P. Wilkinson, B. Wang, J. B. West, M. J. Citardi, K. H. Manwaring, and R. Khadem, "Implementation, calibration and accuracy testing of an image-enhanced endoscopy system," *IEEE Trans. on Medical Imaging*, vol. 21, no. 12, pp. 1524–1535, 2002.

[12] T. Yamaguchi, M. Nakamoto, Y. Sato, K. Konishi, M. Hashizume, N. Sugano, H. Yoshikawa, and S. Tamura, "Development of a camera model and calibration procedure for oblique-viewing endoscopes," *Computer Aided Surgery*, vol. 9, no. 5, pp. 203–214, 2004.